AIAA Paper 98-0606, 36th AIAA Aerospace Sciences Meeting

WIND TUNNEL MEASUREMENTS OF PARAFOIL GEOMETRY AND AERODYNAMICS

C. Matos[†], R. Mahalingam[†], G. Ottinger[¥] , J. Klapper[¥], R. Funk[#] and N. Komerath[*]
School of Aerospace Engineering
Georgia Institute of Technology
Atlanta, GA 30332-0150

ABSTRACT

Video-based photogrammetry combined with a laser sheet is used to measure the section profiles of a parafoil model of aspect ratio 2.5 during tethered testing in a low-speed tunnel. Surface contours of parafoils during operation in a wind tunnel are obtained. Leading-edge collapse, high angle of attack flight, and oscillatory yaw are studied. Force measurements, including C_L and C_D for the parafoil, are also obtained for the conditions studied.

INTRODUCTION

The NASA X-38 Experimental Crew Recovery Vehicle uses a parafoil during the final stage of the landing approach. The parafoil is deployed in subsonic flight, guided by the Global Positioning System, and approaches a landing site, facing into the wind. With a final landing flare, the air speed can be reduced to a few feet per second, so that in the presence of a moderate wind speed, soft touchdown can be achieved. This paper studies aerodynamic issues involved in the deployment and operation of such a parafoil.

The parafoil poses an interesting challenge to the aerodynamics researcher. The surface shape is determined by the pressure distribution in and around the parafoil, the porosity of the fabric, and the presence of cell cross-flow, in addition to the fabric structure and the tensions in the lines at the attachment points. The pressure distribution in turn depends on the attitude and the surface shape. Computing the trajectory of such a configuration from first principles poses a very substantial challenge. The first issue we address is the problem of measuring the precise surface shape of the parafoil, and how it changes with model attitude (which is controlled by line tension and line length), model dynamics, and dynamic pressure.

Secondly, there are several interesting issues in the transient phases of the operation. Deployment is an event with multiple time scales. There are substantial time scales involved in changing angle of attack, and the process of high angle-of-attack stalling appears to be somewhat different from what is expected over rigid wings. The behavior at transient negative angles of attack poses difficulties. Again, realistic wind tunnel simulations of these conditions call for a systematic progression of experiments, where the individual processes can be captured and understood.

PREVIOUS WORK

Ware and Hassell (Ref. 1) conducted tests of tethered parafoils at the Langley 30ft x 60ft low speed wind tunnel. The models were double-membrane wings with rectangular planforms and airfoil cross-sections with open leading edges. Two series of tests were conducted: one with wing area kept constant and the other with wing chord kept constant. A full-scale model of aspect ratio 1.5 was also tested. The models were effectively flown in tethered flight from a strain-gage balance. A center-post apparatus was used to provide partial restraint of the constant-area models for measurement of the stability and control characteristics. The models were statically, longitudinally and laterally stable about the confluence point of the suspension lines.

[†] Graduate Research Assistant, Student Member, AIAA
[´] Undergraduate Student
[#] Research Engineer, Member, AIAA
[*] Professor, Associate Fellow, AIAA

Goodrick (Ref. 2) developed an analysis of static and dynamic longitudinal stability of high-performance gliding airdrop systems. The analytical model assumed a two-mass, rigidly connected system where the system center of mass was fixed with respect to both the canopy and the cargo. The rigid connection precluded second-order effects of independent pitching oscillations of the canopy and cargo. The static and dynamic longitudinal stability characteristics of parafoils and inflatable wings were computed. He showed that for heavy payloads, the influence of canopy air mass may cause significant adverse dynamics.

Goodrick (Ref. 3) extended the work of Ref. 2 to a 6-d.o.f simulation, and discussed scale effects evident from experimental data, on tilt and turn rates, and phugoid characteristics. Lingard (Ref. 4) presented a semi-empirical model for the aerodynamics of ram air parachutes, with particular interest in swept-wing closed-cell versions. Low aspect ratio wing theory was used to establish the model and derive the glide performance of the ram air parachute. Optimum lift-to-drag ratio was shown to be close to be 3:1, in agreement with practical observations. Increases in aspect ratio were found to generate added line drag which offset the gains in aerodynamic efficiency. The model suggested that closing the leading edge by using a swept leading edge would enable glide ratios of 3:1.

Brown (Ref. 5) studied testing techniques to measure the performance of full-scale parafoils. The parafoil was tethered to a truck. Measurements of the airspeed, tether tension and tether angle were used to determine the lift-to-drag ratio and lift coefficient. A bubble level, airspeed indicator and load cell readout were mounted to a protractor board, and viewed using a video camera. A pyramid structure protected the test instruments by limiting the tether cable angle. The parafoil was controlled using steering lines by an operator standing in front of the test fixture to keep the parafoil above the truck. A release mechanism was provided to protect against severe gust loads, capable of overturning the truck. Data from the video tape were averaged over 60 video images from a 2-second segment of data to remove random noise.

Geiger and Golden (Ref. 6) performed tests on three high-fidelity parafoil models at the 80’ x 120’ test section of the National Full-Scale Aerodynamic Complex at NASA Ames Research Center. The models ranged in wing area from 350 to 1200 ft^2 and aspect ratios from 1.7 to 3.9. Aerodynamic data were obtained for ranges of parameters including wing size, airfoil section, aspect ratio, suspension line geometry, anhedral ratio, and control response. The models were verified to be statically stable at all aspect ratios, dynamic pressures and angles of attack up to stall. The maximum lift-to-drag ratio was 4.4.

PRESENT SCOPE OF WORK

The previous work on parafoils is seen above to include several efforts to model the stability and dynamics of systems, to consider the effects of scale, and several large wind tunnel model tests and outdoor full-scale tethered tests to study parametric variations. To reduce uncertainty in the system design, and provide tools to improve the designs, these diverse sources of information have to be integrated and linked to first-principles-based systematic flow calculations, and dynamic simulations. Three problems of interest are identified and attacked here:

1. Acquisition of a closed-form set of data on a model parafoil in the wind tunnel, including data on forces and the precise surface geometry as a function of model attitude and the effects of control deflections.

2. Capture of transient events such as the collapse of the leading edge of the parafoil at low angle of attack, and identification of the processes which cause this.

3. Capture of the high angle-of-attack stalling mechanism.

The above items are needed to validate calculation methods where the surface shape has to be prescribed initially, and then computed from the fabric properties and the dynamic pressure and inlet attitude. High accuracy is needed in specifying the test condition and the surface geometry. Thus a high priority in the work to-date has been the development of a capability to perform photogrammetry in the windtunnel during steady and unsteady operation of the parafoil, the latter to be performed by capturing views of the model at the same instant from video frames acquired using several video cameras.

The tests described here were the first tunnel entry for this multi-faceted experiment.

Among the issues faced are those of stabilizing the parafoil at various test conditions, including the effects of operating the yaw and roll controls.

Due to the relatively small tunnel size (7' x 9') the attachment system had to be developed to permit stable attachment of the parafoil model, while at the same time permitting force measurement. This was done using a set of miniaturized strain gages which were attached to the tension lines holding the parafoil.

PHOTOGRAMMETRY TECHNIQUE

Meyn and Bennett (Ref. 7) developed a low-cost, video imaging system for three dimensional stereo ranging, and used the technique to determine angle of attack for a large scale parafoil. In the present experiments, surface geometry and angle of attack of a small scale parafoil are determined using this technique. Stereo ranging, or photogrammetry, allows the measurement of three-dimensional positions from flow visualization, as well as position and deflections of structures under aerodynamic loading. The photogrammetry technique is discussed in more detail in the Appendix.

There are two major sources of error in this method. The first is the fact that the method does not take into account any distortion of the images due to the cameras' lenses. The second is possible error in measuring the calibration points. The first issue has not been addressed in this experiment. The second can be minimized by maximizing the accuracy of the measurement of the calibration grid positions.

EXPERIMENTAL SETUP

A multi-celled, aspect ratio 2.5 parafoil with a chord length of 0.635 m was suspended upside-down from the ceiling of the 7x9 foot test section of the Harper windtunnel at Georgia Tech. Orienting the parafoil upside-down made deployment automatic when the tunnel speed reached approximately 4.6 m/s, and increased the stability of the parafoil. Multiple attachment lines on the parafoil converged to two points, where the miniature tension/compression force transducers were attached. Cameras recorded the angles of the two main lines for the parafoil, so that the recorded forces could be resolved into lift and drag.

For surface geometry determination, an irregular calibration grid of nine 1.25 cm diameter clay balls was suspended from the ceiling. Using nine calibration points made the calibration matrix overdetermined. These balls covered the approximate area in which the parafoil would fly. The location of the balls in (x, y, z) space was then carefully measured from an arbitrarily chosen zero. Four video cameras were placed around the parafoil on stationary tripods as shown in Figure 1. Two cameras were placed upstream of the parafoil, and two behind. Cameras were not placed to the sides of the parafoil due to space limitations. The entire surface of interest was covered by at least two cameras, and most of the parafoil's upper surface could be seen with all four cameras. Like the calibration matrix, the transform matrix was overdetermined for any points with data from more than two cameras. The calibration grid was recorded by all four cameras with the parafoil removed from the test section. The grid was then removed and replaced with the parafoil.

The parafoil was suspended from the ceiling of the tunnel at the collocation points using 20 lb_f load cells as illustrated in Fig. 2. Various control line setups were used to vary the parafoil's attitude in the tunnel. Setup 1 used three control lines at the outer panels of each wing pulled together to provide a flap deflection on the parafoil. Setup 2 used these same lines pulled rearward and upward to increase the parafoil angle of attack. Using only one line in this setup created yawing moment on the parafoil. Setup 3 used lines attached at the front, lower surface of the parafoil to pull the parafoil to a lower angle of attack and study lip collapse. In each setup the control lines were instrumented with 10 lb_f load cells to measure the tension in each line. The tension force in each line was monitored and recorded using an A/D board in a PC which also monitored tunnel speed. Before each run a wind-off tare was taken to remove the weight of the parafoil and any lines. The tunnel was then brought up to speed and force data was recorded.

Miniature video cameras were used to measure the angles of the lines at the collocation points and the angles of any control lines to provide the geometric angles necessary to resolve force directions. An angle board was recorded behind the lines before the force runs for reference in the angle reduction process. The line angles were found by grabbing frames from the video and measuring the angle of the lines using the angle

board frame as a reference. These angles were then used to resolve the line forces measured into lift and drag generated by the parafoil. Figure 3 shows a grabbed image of the lines at the collocation points and the angles measured. Symmetry was assumed here, so the angle of only one of the each of the main and control lines was recorded. For force and surface geometry measurements, the parafoil was flown at a tunnel speed of 40 ft/sec.

Surface geometry was obtained in all cases by simply recording the parafoil with each of the four cameras, using a framer grabber to acquire images from the videotape, and using a post-processing code to determine the actual surface geometry. The photogrammetry technique requires that the same point in space be located on all camera images. In order to accomplish this, a coarse grid was marked on the parafoil. This allowed for multiple chordlines of data points to be obtained, from which the surface geometry of the parafoil could be reconstructed. Where grid lines intersected, the same point on all cameras could easily be determined. In addition, for the unrestrained flight case, where the parafoil was in very steady flight, a laser sheet was traversed across the span of the parafoil. A large number of intersections between the laser sheet and the gridlines across the span of the parafoil could be formed as the laser sheet traverses across the parafoil. A large number of surface geometry points could be determined without a large number of gridlines on the parafoil itself. For unsteady flight conditions, since the location of the parafoil varies with time, points could only be determined from the gridlines on the parafoil obtained from corresponding frames of video, so fewer points were obtained.

RESULTS

1. Free Flight

The surface geometry technique was first used on the unrestrained parafoil case. Through the surface geometry results, the angle of attack of the parafoil was found to be 8.8°, as measured from leading edge to trailing edge. The parafoil section is compared to the Clark Y airfoil in Fig. 4. The parafoil shows less curvature on the back half of the chordline than the Clark Y.

Force measurements were also made on the parafoil in free flight. The parafoil had a line length to span ratio of approximately 0.55. For free flight, the parafoil averaged an L/D of 3.1. This is a little higher than the reported value of 2.8 for the $300m^2$ parafoil with a similar line length to span ratio reported by Lingard (Ref. 8). A smaller $36m^2$ parafoil had a slightly higher L/D ratio of 3.25. Values vary widely because of the differences in line drag which depends on length and number of the lines and the line diameter. C_L for the parafoil tested in this experiment was found to be 0.45 in free flight, with a C_D of 0.14.

2. Flap Variation

The angle of attack when maximum flap was applied was determined from the photogrammetry results to be 6°. Adding flap in this case caused a decrease in the angle of attack. The flap was formed at the ends of the span of the parafoil, rather than the center. Because of this method of flap formation, the area of the surface geometry covered by the cameras does not show a significant change in slope of the parafoil near the trailing edge. Figure 5 shows a comparison between the surface geometry determined for the flapped case, and that of the free flight case. Other than the change in angle of attack, there is little difference in the parafoil sections. As in the free flight case, force measurements were taken for a range of flap deflections. Figure 6 shows the variation of C_L with C_D. C_L increases from 0.54 to 0.8 and C_D increases from 0.22 to 0.38 as the flap angle increases. For the flapped parafoil case, L/D diminished to 2.1 as soon as the flap was formed, and remained close to constant as the flap angle was increased.

3. Angle of Attack Variation

The angle of attack of the parafoil was changed next, in an attempt to capture the high angle of attack stalling mechanism. Due to the steady state nature of the flow, we were unable to observe the unsteady phenomenon of stall. The maximum angle of attack achieved was 14°, an increase of just over 5 degrees from the baseline flight angle of attack. Surface geometry was obtained for a few chordlines in this case. Fig. 7 shows a comparison of the increased angle of attack case with the free flight parafoil. The front of the parafoil is seen to flatten out slightly, but that is the only change, other than the increase in angle of attack, from the free flight case. Force measurements were also made for this case for the range of angle of attacks from free flight (8.8°) to

maximum angle of attack (14°). The L/D for the increased angle of attack was approximately 3.0, and remained constant over the range of angles traversed. C_L and C_D values were similar to those for the free flight case, at 0.44 and 0.14, respectively.

4. Yawing

Both left and right yawing moment cases were examined as well. For the right side yaw case, most of the parafoil moved out of the field of view of the video cameras, so only one chordline was obtained. The parafoil was observed to fly at an angle to the freestream, but insufficient surface geometry was obtained to determine the angle. As the force on the parafoil increased, unsteady spanwise oscillations began, causing the parafoil to collide with the ceiling of the windtunnel. Surface geometry reconstruction of the portion of the parafoil still in the field of view determined the angel of attack to be 6°. For yawing moment on the left side of the parafoil, surface geometry determined the angle of attack to be 8°. As in the previous yawing case, the parafoil was seen to fly at an angle to the freestream. In this case, enough of the surface geometry was seen in order to determine the yaw angle to be 3.5°. Unstable side to side oscillations were also induced when a high amount of force was applied. Force measurements were also taken for both yaw cases. The L/D ratio for both cases averaged 3.1. Yawing moment was seen to have little effect on the L/D ratio, as it remained the same as for the free flight case. C_L and C_D values were the same as for the free flight case as well.

5. Lip Collapse

The lip collapse phenomenon was the last flight condition tested. The parafoil's angle of attack was slowly decreased in steps until the lip collapsed. This was seen at an angle of attack of -3°, as determined from the photogrammetry results. The rear of the parafoil is seen to deflate first, as indicated by the chordlines collapsing into towards the center at the rear of the parafoil, instead of remaining parallel to each other, as shown in Fig. 8. Force measurements show the L/D ratio to decrease from 2.8 to 2.0 as the lip progressively collapses. Figure 9 shows the variation in C_L verses C_D as the angle of attack is decreased. C_L increases from 0.47 to 0.71 as C_D increases from 0.16 to 0.34.

Figure 10 shows a time lapse sequence of the collapse of the parafoil's lip. The parafoil begins flying in the usual steady state flight. The angle of attack is slowly decreased by small increments. At a low enough angle of attack, the edge of the lip of the parafoil in the center begins to fold down. If the angle of attack is further decreased, more of the lip folds down, and the folding expands outwards along the span. If the angle of attack is increased again, it is possible to recover from this phenomenon, if the lip has not collapsed too much. As more of the lip collapses, the effective inlet height decreases further. If the inlet height becomes too small, the inlet no longer covers the range of movement of the stagnation streamline (Ref. 8). The stagnation point moves onto the upper surface of the lip, collapsing it further. The parafoil starts to deflate, and oscillatory behavior begins. This folds the lip down further due to the increased pressure on the folded lip of the leading edge. Oscillations begin and increase in amplitude as the lip collapses further. This process is extremely unsteady, and the parafoil eventually collapses entirely. Once violent oscillations have begun, it is almost impossible for the parafoil to recover. This behavior was seen in two different parafoils with aspect ratio 2.5.

6.Error in Photogrammetry Technique

To gain an idea of the amount of error in the surface geometry reconstruction, the location of each of the calibration points was determined using a calibration grid of the remaining eight points. Most of the coordinates were correctly determined to within 0.48 cm in each direction. Two points, however, had larger errors. This is most likely due to either a) localized distortion in the camera lens of one or more of the video cameras, or b) inaccurate measurement of the true position of the two points. Due to the over-determination of the calibration coefficients, though, the error in the two grid points does not have a large effect on the results. The results for several free flight chords were changed by less than 0.38 cm in each direction with the removal of points 6 and 9, with the majority of the differences being on the order of 0.13 cm. Interestingly, the anticipated problem of "fish-eye" distortion in the camera lenses was not observed.

7. Reconstruction of Surface Geometry

The usefulness of the photogrammetry technique can be seen in Fig. 11, which shows the three dimensional reconstruction of a section of the parafoil geometry in free flight. This three-dimensional reconstruction can easily be converted into a three dimensional grid for use in CFD codes. The plot corresponds very well to the shape seen directly on the videotapes.

CONCLUSIONS

The L/D ratio of 3.1 in free flight for the 2.5 aspect ratio parafoil tested, with a 0.55 line length to span ratio, was found to agree with previously published results. The L/D ratio was seen to decrease when flap was added, but was not effected by yawing conditions or increases in angle of attack.

The photogrammetry technique was demonstrated to be useful in tracking geometry changes during transient maneuvers as well as during steady state flight. The technique was found to work well to determine the surface geometry of the upper surface of the parafoil. The results from this technique can be used to validate CFD code prediction of surface shape or used as input to lower fidelity codes for performance estimation. A better three dimensional model of the parafoil can also help in determining three dimensional effects.

The occurrence of lip collapse at low angles of attack was found to be a repeatable process over different parafoils, with a predictable progression of events leading to total collapse.

The accuracy of the photogrammetry technique could be increased by more accurately measuring the locations of the calibration points. Using a grid with a larger number of points would help better determine the accuracy of the method, as well as the optimal number of points to use.

ACKNOWLEDGEMENTS

This work was performed under a grant from NASA Johnson Space Center. The technical monitor is Richard Barton.

REFERENCES

1. Ware, G.M., Hassell, J.L., “Wind-Tunnel Investigation of Ram-Air-Inflated All-Flexible Wings of Aspect Ratios 1.0 to 3.0”. NASA TM SX-1923, Langley Research Center, Hampton, VA, 1969.

2. Goodrick, T.F., “Theoretical Study of the Longitudinal Stability of High-Performance Gliding Airdrop Systems”. AIAA Paper 75-1394, 5th Aerodynamic Decelerator Systems Conference, 1975.

3. Goodrick, T.F., “Scale Effects on Performance of Ram Air Wings”. AIAA Paper 84-0783, January 1984.

4. Lingard, S., “The Aerodynamics of Gliding Parachutes”. AIAA-86-2427-CP, 9th Aerodynamic Decelerator and Balloon Technology Conference, October 1986.

5. Brown, G.J., “Tethered Parafoil Test Technique”. AIAA 89-0903-CP, January 1989.

6. Geiger, R.H., and Golden, R.A., “Advanced Recovery Systems Wind Tunnel Test Report - Series 2 - Vol. 1 - 3, Pioneer Aerospace Corporation, Melbourne, FL, August 1990.

7. Meyn, L.A., and Bennett, M.S., “A Two Camera Video Imaging System With Application to Parafoil Angle of Attack Measurements”. AIAA Paper 91-0673, Jan. 1991.

8. Lingard, S., “Precision Aerial Delivery Seminar Ram-Air Parachute Design”, 13th AIAA Aerodynamic Decelerator Systems Technology Conference, May 1995.

FIGURES

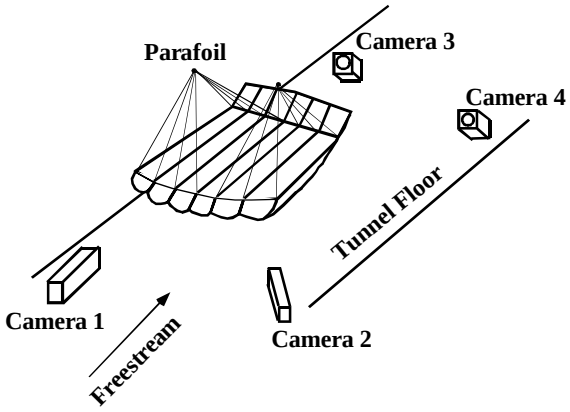

Figure 1: Configuration for parafoil surface geometry measurement.

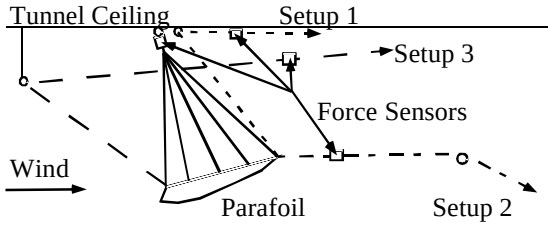

Figure 2: Schematic for changing flap, angle of attack and yaw of parafoil.

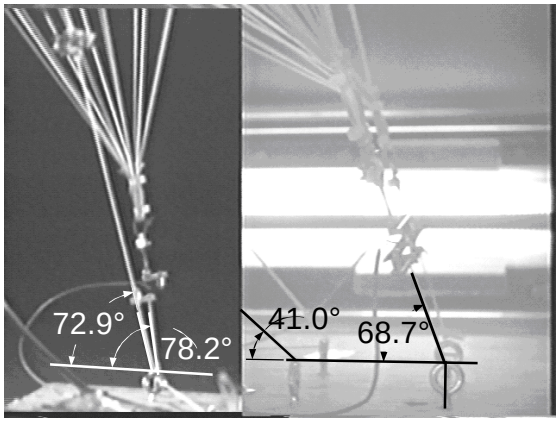

Figure 3: Demonstration of angle determination for force lines.

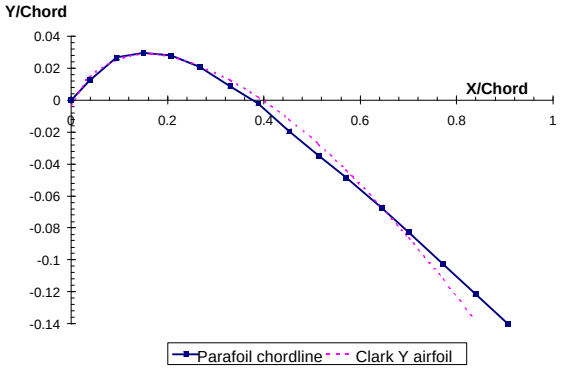

Figure 4: Comparison of Clark Y airfoil section and measured parafoil geometry in steady state unrestrained flight.

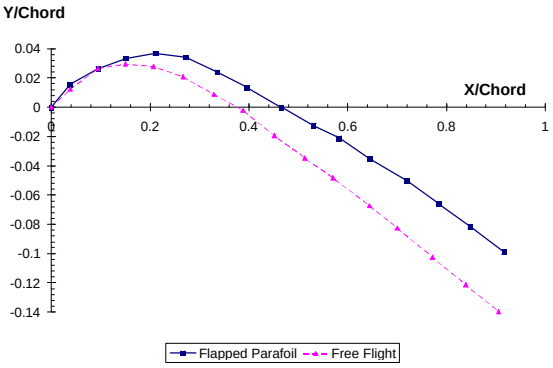

Figure 5: Comparison of flapped and free flight parafoil sections

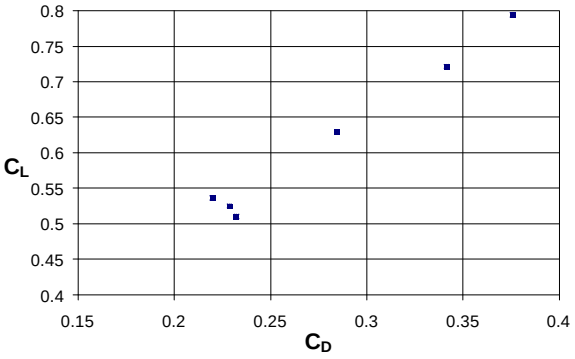

Figure 6: C_L vs. C_D for flapped parafoil.

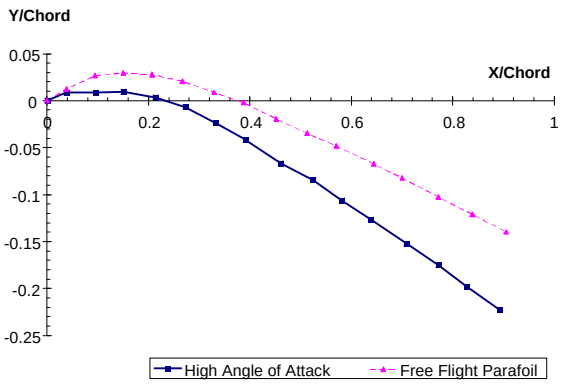

Figure 7: Comparison of angle of attack and free flight parafoil cases.

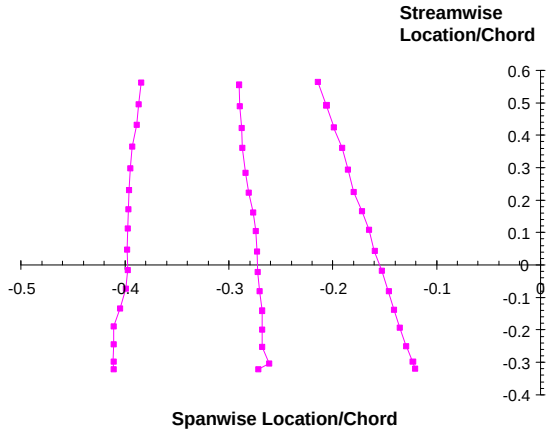

Figure 8: Chordlines of parafoil with collapsed lip, as seen from above the parafoil's upper surface.

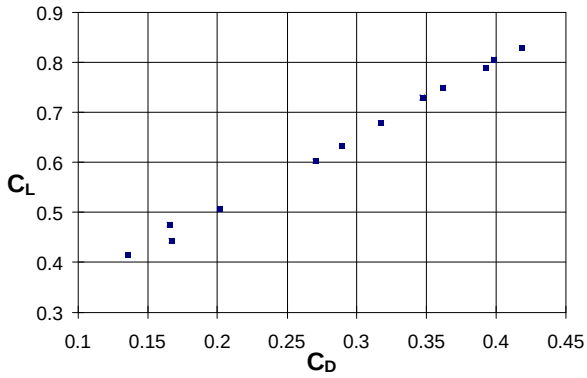

Figure 9: C_L versus C_D for leading edge collapse over range of angle of attacks.

Figure 10: Time sequence of leading edge collapse process.

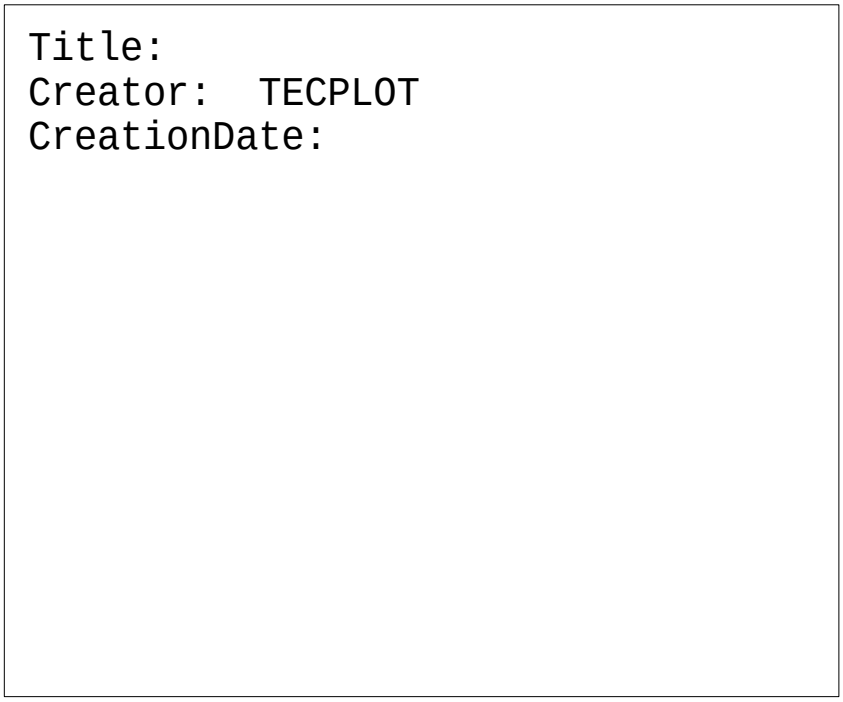

Figure 11: Three-dimensional recreation of parafoil surface geometry in free flight.

APPENDIX

The photogrammetry technique developed by Meyn and Bennett (Ref. 7) approximates the camera images as "line-of-sight" projections of the object or flow visualization onto image planes. A point at real world location (X_w, Y_w, Z_w) is projected onto the image plane of the camera at (X_n,Y_n). If the exact position and orientation of each camera is known, the real world position of the point can be determined from trigonometry relationships. However, precisely measuring the orientation and location of the cameras can be difficult. The method of photogrammetry instead uses a generalized matrix model to form a "map" from the camera image planes back to the real world coordinate system.

Calibration points are used to provide known locations in real space that correspond to certain known locations in the camera image planes. The cameras must all contain the calibration points within their viewfield. For each calibration point with real world position $\left(X_w^n, Y_w^n, Z_w^n\right)$, each camera "sees" the point on its image plane at a unique location (X_n, Y_n). Through the use of calibration points, the coefficients that make up the transformation matrix can be determined. For each calibration point, an equation can be written that relates the known real world position of the point to the known image location on the camera image plane. For each camera, equations of the following form are solved:

$$\left(c_{11}X_w^n + c_{12}Y_w^n + c_{13}Z_w^n + c_{14}\right) - X_n\left(c_{31}X_w^n + c_{32}Y_w^n + c_{33}Z_w^n\right) = X_n$$
$$\left(c_{21}X_w^n + c_{22}Y_w^n + c_{23}Z_w^n + c_{24}\right) - Y_n\left(c_{31}X_w^n + c_{32}Y_w^n + c_{33}Z_w^n\right) = Y_n$$

where (X_n,Y_n) is the location of the n^{th} calibration point in the camera's image plane, and c_{ij} are the unknown calibration coefficients for that camera. This can be rewritten into matrix form as:

$$\begin{bmatrix} X_w^1 & Y_w^1 & Z_w^1 & 1 & 0 & 0 & 0 & 0 & -X_1X_w^1 & -X_1Y_w^1 & -X_1Z_w^1 \\ 0 & 0 & 0 & 0 & X_w^1 & Y_w^1 & Z_w^1 & 1 & -Y_1X_w^1 & -Y_1Y_w^1 & -Y_1Z_w^1 \\ \cdots & \cdots & \cdots & \cdots & \cdots & \cdots & \cdots & \cdots & \cdots & \cdots & \cdots \\ \cdots & \cdots & \cdots & \cdots & \cdots & \cdots & \cdots & \cdots & \cdots & \cdots & \cdots \\ X_w^n & Y_w^n & Z_w^n & 1 & 0 & 0 & 0 & 0 & -X_nX_w^n & -X_nY_w^n & -X_nZ_w^n \\ 0 & 0 & 0 & 0 & X_w^n & Y_w^n & Z_w^n & 1 & -Y_nX_w^n & -Y_nY_w^n & -Y_nZ_w^n \end{bmatrix} \begin{pmatrix} c_{11} \\ c_{12} \\ c_{13} \\ c_{14} \\ c_{21} \\ c_{22} \\ c_{23} \\ c_{24} \\ c_{31} \\ c_{32} \\ c_{33} \end{pmatrix} = \begin{pmatrix} X_1 \\ Y_1 \\ \vdots \\ \vdots \\ X_n \\ Y_n \end{pmatrix}$$

For each camera there are eleven unknowns, so at least six calibration points must be used, since each calibration point provides two equations. A least squares method can be used to solve the resulting over-determined set of linear equations if more points are used.

Each camera has its own unique set of eleven calibration coefficients. Once the coefficients have been determined for each of the cameras, a matrix to solve for the world coordinate vector (X_w, Y_w, Z_w) from the image vectors of the same point the cameras can be formed. At least two cameras are required to solve the system. For illustrative purposes, the equation below is written for four cameras, with image point locations of (X_{c1}, Y_{c1}), (X_{c2}, Y_{c2}), (X_{c3}, Y_{c3}), and (X_{c4}, Y_{c4}).

$$\begin{bmatrix} \left(X_{c1}c_{31}^1 - c_{11}^1\right) & \left(X_{c1}c_{32}^1 - c_{12}^1\right) & \left(X_{c1}c_{33_{33}}^1 - c_{13}^1\right) \\ \left(Y_{c1}c_{31}^1 - c_{21}^1\right) & \left(Y_{c1}c_{32}^1 - c_{22}^1\right) & \left(Y_{c1}c_{33}^1 - c_{23}^1\right) \\ \left(X_{c2}c_{31}^2 - c_{11}^2\right) & \left(X_{c2}c_{32}^2 - c_{12}^2\right) & \left(X_{c2}c_{33}^2 - c_{13}^2\right) \\ \left(Y_{c2}c_{31}^2 - c_{21}^2\right) & \left(Y_{c2}c_{32}^2 - c_{22}^2\right) & \left(Y_{c2}c_{33}^2 - c_{23}^2\right) \\ \left(X_{c3}c_{31}^3 - c_{11}^3\right) & \left(X_{c3}c_{32}^3 - c_{12}^3\right) & \left(X_{c3}c_{33}^3 - c_{13}^3\right) \\ \left(Y_{c3}c_{31}^3 - c_{21}^3\right) & \left(Y_{c3}c_{32}^3 - c_{22}^3\right) & \left(Y_{c3}c_{33}^3 - c_{23}^3\right) \\ \left(X_{c4}c_{31}^4 - c_{11}^4\right) & \left(X_{c4}c_{32}^4 - c_{12}^4\right) & \left(X_{c4}c_{33}^4 - c_{13}^4\right) \\ \left(Y_{c4}c_{31}^4 - c_{21}^4\right) & \left(Y_{c4}c_{32}^4 - c_{22}^4\right) & \left(Y_{c4}c_{33}^4 - c_{23}^4\right) \end{bmatrix} \begin{pmatrix} X_w \\ Y_w \\ Z_w \end{pmatrix} = \begin{bmatrix} c_{14}^1 - X_{c1} \\ c_{24}^1 - Y_{c1} \\ c_{14}^2 - X_{c2} \\ c_{24}^2 - Y_{c2} \\ c_{14}^3 - X_{c3} \\ c_{24}^3 - Y_{c3} \\ c_{14}^4 - X_{c4} \\ c_{24}^4 - Y_{c4} \end{bmatrix}$$

Here, the calibration coefficients for different cameras are distinguished by different superscripts. Additional cameras are easily accommodated by adding an addition two equations to the matrix for each camera. This matrix is also now overdetermined. The Singular Value Decomposition method can be used to solve the system for the real world position (X_w, Y_w, Z_w).